Vicinal interface sensitive magneto-optical Kerr effect: Application to Co/Au(322)

J. Hamrle
Laboratoire de Physique des Solides, UMR CNRS 8502, Université Paris XI, 91405 Orsay, France
and Institute of Physics, Charles University, Ke Karlovu 5, 12116 Praha 2, Czech Republic

J. Ferré* and J. P. Jamet
Laboratoire de Physique des Solides, UMR CNRS 8502, Université Paris XI, 91405 Orsay, France

V. Repain
Laboratoire de Physique des Solides, UMR CNRS 8502, Université Paris XI, 91405 Orsay, France
and Groupe de Physique des Solides, UMR CNRS 7588, Univ. Paris 7 et Paris 6, 75251 Paris, France

G. Baudot and S. Rousset
Groupe de Physique des Solides, UMR CNRS 7588, Univ. Paris 7 et Paris 6, 75251 Paris, France
(Received 12 December 2002; published 28 April 2003)

Vicinal interface sensitive magneto-optical Kerr effect (VISMOKE) is predicted for ferromagnetic films deposited on stepped (e.g., vicinal) substrates. VISMOKE originates from the interference between optostructural and magneto-optical perturbations at stepped interface. The contribution of VISMOKE to total Kerr effect is calculated for any magnetization orientation and arbitrary incidence angle of light. Predictions on the variation of VISMOKE with sample rotation around its normal axis is probed by an ultrathin Co film deposited on a high quality Au(322) vicinal surface. The calculated optostructural interface perturbation is consistent with its experimental value.

DOI: 10.1103/PhysRevB.67.155411 PACS number(s): 75.70.−i, 78.20.Ls

I. INTRODUCTION

During last decade many effort has been made to relate the magnetism to the structure in ultrathin ferromagnetic (FM) films.[1,2] However, the knowledge of the magnetism at buried interfaces is still a challenge. Only few techniques, such as the magneto-optical second harmonic generation[3] or x-ray magnetic circular dichroism,[4] can give such informations in some cases. Up to now, only a few experiments have been carried out on films deposited on vicinal interfaces in spite of the well-known structure of the involved interface that may be considered as a test bed for basic studies. In particular, the step-induced magnetic anisotropy of FM films may be well controlled.[5] Stepped substrates can be also used to drive anisotropic magnetic domain-wall propagation[6] that could be of interest for applications.

The magnetic properties of ultrathin films are commonly probed by magneto-optics. In this paper, we show that a nontrivial different magneto-optical Kerr effect (MOKE) is expected as the consequence of the low symmetry of the vicinal interface. This vicinal interface sensitive MOKE (VISMOKE) is shown to be related to the in-plane component of the magnetization and can be detected even at normal light incidence ($\varphi=0$). No MOKE signal, proportional to the magnetization, is usually expected in this MO configuration for flat surfaces.[7] In the ultrathin film approximation[8] a convenient approach is introduced here to calculate MOKE, including VISMOKE contribution for arbitrary light incidence and magnetization orientation. We show that VISMOKE originates from the interference between optostructural and first-order magneto-optical perturbations at the interface. Such an effect was recently predicted by Pethukov *et al.*[9] for low symmetry surfaces and qualitatively discussed for vicinal interfaces.

Here, VISMOKE is evidenced experimentally for an ultrathin FM Co film, deposited on a Au vicinal surface. Furthermore, from either MOKE or reflectivity measurements, we deduce independently the value of the step induced optostructural perturbation. Finally, this optostructural perturbation at vicinal surface is estimated from a simple analytic electromagnetic model. The agreement with the experimental values is good and, for weak vicinality, VISMOKE is predicted to vary linearly with the step density.

II. ANALYTICAL EXPRESSION OF MOKE AND VISMOKE

Let us note $(\hat{x},\hat{y},\hat{n})$ and $(\hat{X},\hat{Y},\hat{n})$, the Cartesian referentials for the light and the sample, respectively [Fig. 1(a)]. The plane of incidence of the light is $\hat{y}\hat{n}$. The only symmetry element of the vicinal interface is a $\hat{X}\hat{n}$-mirror plane, the $\hat{X}$ axis being perpendicular to the step edges and $\hat{n}$ normal to the film. When rotating the sample around $\hat{n}$, the orientation of vicinal steps with respect to the light referential is determined by the angle $\alpha=(\hat{x},\hat{X})$. The orientation of sample magnetization is given by angles β and γ in the *light* referential [Fig. 1(b)].

The optical properties of the FM layer are described by the complex permittivity tensor $\bar{\bar{\varepsilon}}$, so that $\mathbf{D}=\varepsilon_0\bar{\bar{\varepsilon}}\mathbf{E}$, where ε_0 is the vacuum permittivity. In general, the element ε_{ij} $(i,j=x,y,z)$ of the permittivity tensor $\bar{\bar{\varepsilon}}$ can be decomposed into structural (i.e., nonmagnetic) $\varepsilon_{\mathrm{str},ij}$ and magnetic $\varepsilon_{\mathrm{mag},ij}$ contributions,

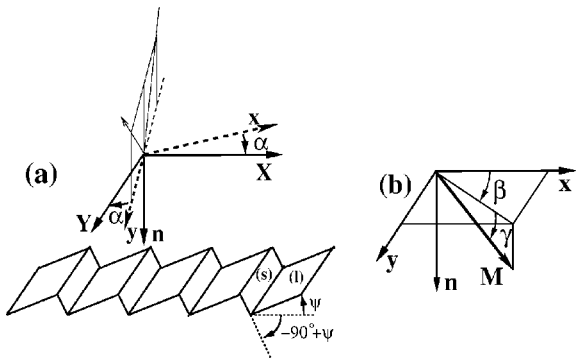

FIG. 1. (a) Light $(\hat{x},\hat{y},\hat{n})$ and sample $(\hat{X},\hat{Y},\hat{n})$ Cartesian referentials. α is the angle of rotation of the sample around $\hat{n}$. (b) Sample magnetization **M** orientation with respect to the *light* referential.

$$\bar{\bar{\varepsilon}}=\bar{\bar{\varepsilon}}_{\mathrm{str}}+\bar{\bar{\varepsilon}}_{\mathrm{mag}}. \tag{1}$$

As follows from Onsager relations of reciprocity, in the absence of magnetic field, the permittivity tensor is symmetrical, i.e., $\varepsilon_{\mathrm{str},ij}=\varepsilon_{\mathrm{str},ji}$.[10]

Because $\bar{\bar{\varepsilon}}$ is a second-rank polar tensor and the vicinal interface has point symmetry group *m* (one mirror axis symmetry), the general form of the structural permittivity tensor for step edges in the plane of incidence ($\alpha=0$) is[11]

$$\bar{\bar{\varepsilon}}_{\mathrm{str}}=\begin{pmatrix}\varepsilon_{11} & 0 & \varepsilon_s\\ 0 & \varepsilon_{22} & 0\\ \varepsilon_s & 0 & \varepsilon_{33}\end{pmatrix}, \tag{2}$$

where a new off-diagonal optostructural element ε_s appears. As will be shown later, the presence of ε_s induces VISMOKE. From symmetry arguments,[11] ε_s is more generally nonzero for interfaces with the following point symmetry groups: 1, $\bar{1}$, 2, *m*, 2/*m*, i.e., when only inversion and *one* mirror plane symmetry operations are allowed. The coefficient ε_s is assumed to be small as compared to the diagonal elements values, which are assumed to be nearly equal ($\varepsilon_{11}\simeq\varepsilon_{22}\simeq\varepsilon_{33}\simeq\varepsilon_d$). For an efficient symmetry breaking in the vicinity of the vicinal interface at depth *n*, ε_s can be nonzero over few atomic distances from the interface. Thus, for simplicity, we introduce a vicinal memory depth t_s, so that $\varepsilon_s t_s=\int\varepsilon_s(n)dn$. When the sample is rotated by an angle α around the $\hat{n}$ axis [Fig. 1(a)], $\bar{\bar{\varepsilon}}_{\mathrm{str}}(\alpha)$ takes the form

$$\bar{\bar{\varepsilon}}_{\mathrm{str}}(\alpha)=\begin{pmatrix}\varepsilon_{11}\cos^2\alpha+\varepsilon_{22}\sin^2\alpha & \frac{1}{2}(\varepsilon_{11}-\varepsilon_{22})\sin 2\alpha & \varepsilon_s\cos\alpha\\ \frac{1}{2}(\varepsilon_{11}-\varepsilon_{22})\sin 2\alpha & \varepsilon_{22}\cos^2\alpha+\varepsilon_{11}\sin^2\alpha & \varepsilon_s\sin\alpha\\ \varepsilon_s\cos\alpha & \varepsilon_s\sin\alpha & \varepsilon_{33}\end{pmatrix}. \tag{3}$$

Since the magnetic perturbations in $\bar{\bar{\varepsilon}}_{\mathrm{mag}}$ are weak, one may consider that $\bar{\bar{\varepsilon}}_{\mathrm{mag}}$ remains isotropic at first order,[7]

$$\bar{\bar{\varepsilon}}_{\mathrm{mag}}=\begin{pmatrix}0 & \varepsilon_m m_z & -\varepsilon_m m_y\\ -\varepsilon_m m_z & 0 & \varepsilon_m m_x\\ \varepsilon_m m_y & -\varepsilon_m m_x & 0\end{pmatrix}, \tag{4}$$

with $\mathbf{M}/M_s=[m_x,m_y,m_z]=[\cos\gamma\cos\beta,\cos\gamma\sin\beta,\sin\gamma]$, M_s being the saturated magnetization. The complex reflection coefficients $r_{ps},r_{sp},r_{ss},r_{pp}$ of the ultrathin FM layer, sandwiched between infinite non-FM substrate and overlayer are then deduced. The first (second) subscripts stand for the direction of the incident (outgoing) light polarization, parallel (*p*) or perpendicular (*s*) to the plane of incidence, respectively. The optical and magneto-optical properties of the FM layer of thickness t_{fm} are described by the general permittivity tensor $\bar{\bar{\varepsilon}}$ [Eq. (1)]. Assuming valid the ultrathin FM layer approximation, i.e., $4\pi\,\mathrm{Re}(N_{\mathrm{fm}})t_{\mathrm{fm}}\ll\lambda_0$, where N_{fm} is the complex refractive index of the FM layer and λ_0 is the wavelength in vacuum,[8] we found the generalized complex MOKE amplitudes, defined as ratios between reflection coefficients (see the Appendix and Table I),

$$\Phi_s=-r_{ps}/r_{ss}=\varrho_s t_{\mathrm{fm}}(A\varepsilon_{yx}+B\varepsilon_{zx}/\varepsilon_d)-\varrho_s t_s A\varepsilon_{yz}\varepsilon_{zx}/\varepsilon_d,$$

$$\Phi_p=r_{sp}/r_{pp}=\varrho_p t_{\mathrm{fm}}(-A\varepsilon_{xy}+B\varepsilon_{xz}/\varepsilon_d)+\varrho_p t_s A\varepsilon_{xz}\varepsilon_{zy}/\varepsilon_d, \tag{5}$$

where $\varrho_{s,p}$ describe the optical contributions of the substrate and overlayer for an incidence angle φ.

For an infinitely thick substrate and an overlayer of thickness t_{over}, composed of the same material, then $A=iN_z/N_{\mathrm{nf}}$, $B=i(N_{\mathrm{nf}}N_0/\varepsilon_d)\sin\varphi$ and

$$\varrho_{s,p}=\frac{(4\pi/\lambda_0)N_0N_{\mathrm{nf}}\exp[4\pi iN_z t_{\mathrm{over}}/\lambda_0]\cos\varphi}{(N_{\mathrm{nf}}^2-N_0^2)(N_z\cos\varphi\pm N_0\sin^2\varphi)}, \tag{6}$$

where $+$, $-$ in the denominator correspond to ϱ_s, ϱ_p, respectively. N_{nf} and N_0 are the complex optical indices of the non-FM sandwiching material and air, respectively, and $N_z=(N_{\mathrm{nf}}^2-N_0^2\sin^2\varphi)^{1/2}$. The parameters $\varrho_{s,p}$, A, N_z are even functions of the incidence angle φ and are quasiconstant for $\varphi\in\langle-30°;30°\rangle$ region, although B is an odd function of φ varying quasilinearly with φ.

Substituting the permittivity tensor elements ε_{ij} from Eqs. (1), (3), and (4) into Eq. (5), the successive terms in Eq. (5) are interpreted as polar (PMOKE), longitudinal (LMOKE) and new VISMOKE contributions to total Kerr effect. VISMOKE is proportional to ε_s over a vicinal memory depth t_s, although PMOKE and LMOKE are proportional to t_{fm}.

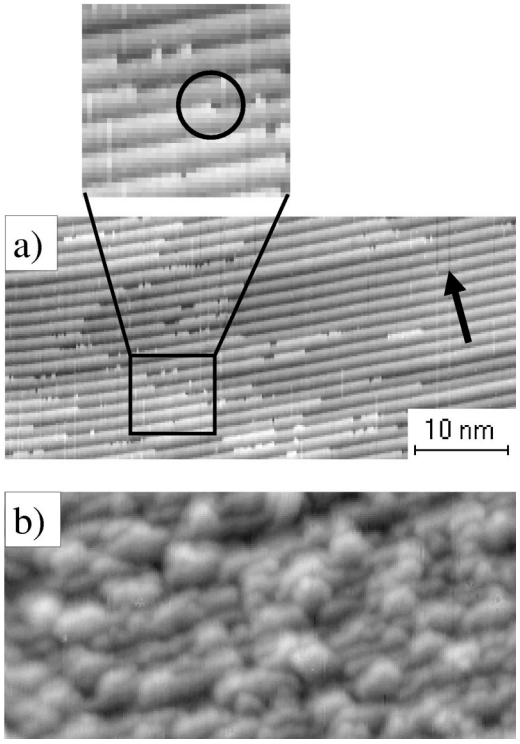

FIG. 2. (a) STM image of the Au(322) vicinal surface. The arrow indicates the $[2\bar{1}\bar{1}]$ descending step direction. The slight azimuthal disorientation induces a secondary steps network (different gray levels). A monoatomic kink is underlined by a black circle on the zoomed image. (b) STM image of 4 AL of Co grown on the Au(322) surface. The image size and orientation are similar to (a).

Hence VISMOKE is an effect linear with magnetization and only sensitive to the vicinal *interface*. Considering, for example, a *s*-MOKE effect Φ_s,

- PMOKE is equal to $\varrho_s t_{\mathrm{fm}} A \varepsilon_m \sin\gamma$, where γ is the disorientation of **M** with respect to the film plane (Fig. 1b).
- LMOKE is equal to $\varrho_s t_{\mathrm{fm}} B(\varepsilon_m/\varepsilon_d)\cos\gamma\sin\beta$. It is maximum when $\mathbf{M}\|\hat{y}$, i.e., when **M** lies at the intersection of the sample plane and of the incidence plane of the light ($\gamma=0,\ \beta=90°$).
- VISMOKE is $-\varrho_s t_s A(\varepsilon_s\varepsilon_m/\varepsilon_d)\cos\gamma\cos(\alpha-\beta)$ and has a more complex behavior due to interference between structural ε_s and magnetic ε_m perturbations. For a fixed orientation of **M** in the light referential ($\beta,\gamma=\mathrm{const}$), the periodicity of VISMOKE with sample rotation α is 2π. This means that a sample rotation of π reverses the sign of VISMOKE.

When **M** is perpendicular to step edges ($\mathbf{M}\|\hat{X}$), VISMOKE is maximum since $(\alpha-\beta)=0$ or 180°. As can be seen from comparison of the first and the third term of Eq. (5) the dependences of VISMOKE or PMOKE on the incidence angle φ are identical.

VISMOKE arises from the cross terms $\varepsilon_{yz}\varepsilon_{zx}$ or $\varepsilon_{xz}\varepsilon_{zy}$. In general, the off-diagonal structural elements of the permittivity tensor can be induced by sample rotation if the diagonal elements ε_{11}, ε_{22}, ε_{33} are slightly different. But, as can be seen from Eq. (3), the structural part of the elements ε_{yz}, ε_{zx}, ε_{xz}, ε_{zy} cannot be induced by sample rotation.

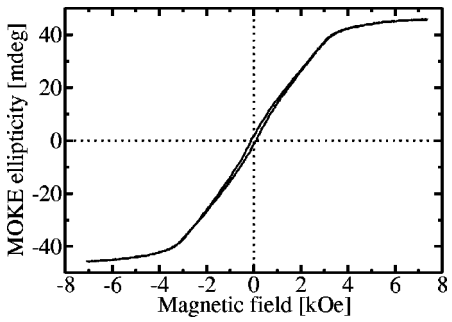

FIG. 3. PMOKE hysteresis loop measured at normal incidence in a field parallel to $\hat{n}$. A small remanent magnetization is measured. The perpendicular anisotropy field is only 3.5 kOe for this 5-AL-thick Co layer deposited on Au(322).

III. SAMPLE PROPERTIES

Magnetic anisotropy favors an out-of-plane orientation of **M** in flat Au/Co(t_{Co})/Au(111) films until a sudden in-plane spin reorientation for a Co thickness $t_{\mathrm{Co}}=10$ atomic layers (AL).[12] The situation is different for films deposited on a Au(322) vicinal surface. In this case, **M** reorients slowly from the out-of-plane to in-plane direction when increasing t_{Co}. Thus to study VISMOKE, a $t_{\mathrm{Co}}=5$ AL was selected in order to get a large enough in-plane magnetic component.

The Au(322) single-crystal substrate is a disk of 4 mm diameter and 2 mm thickness, mechanically polished to a mirrorlike surface. Then the surface is prepared *in situ* in an ultrahigh-vacuum (UHV) chamber with a base pressure of 3×10^{-11} mbar by repeated cycles of Ar^+ sputtering at 900 eV and annealing at 800 K. The Au(322) surface is disoriented by a miscut angle $\psi=11.4°$ [Fig. 1(a)] and is ideally made of 1.17-nm terrace width. All steps are monoatomic, 0.235 nm high [Fig. 2(a)]. The purity of the initial Au surface is checked using Auger electron spectroscopy. Cobalt is evaporated at a low pressure smaller than 2×10^{-10} mbar. Figure 2(b) shows the surface topography after the deposition of a Co layer. Although it is still possible to distinguish locally the vicinal staircase, the Co surface is rough and much more isotropic than the initial Au(322) surface. This is due to the fact that Co does not grow layer by layer since it has a larger surface energy than Au. For this reason, we consider only the Au(322)/Co interface as a symmetry breaking source for the VISMOKE calculations. The 5-AL Co layer is capped with a 7-AL Au overlayer for *ex situ* magneto-optic measurements.

IV. MOKE AND VISMOKE EXPERIMENTAL RESULTS

MOKE ellipticity of the Au(7 AL)/Co(5 AL) film structure deposited on a Au(322) vicinal surface is measured at 1.95-eV photon energy for both polar ($\mathbf{H}\|\hat{n}$) and transverse ($\mathbf{H}\|\hat{x}$) geometries of the external magnetic field **H**. Figure 3 shows the usual PMOKE ellipticity hysteresis loop at normal incidence ($\varphi=0$) for a field **H** applied perpendicular ($\mathbf{H}\|\hat{n}$)

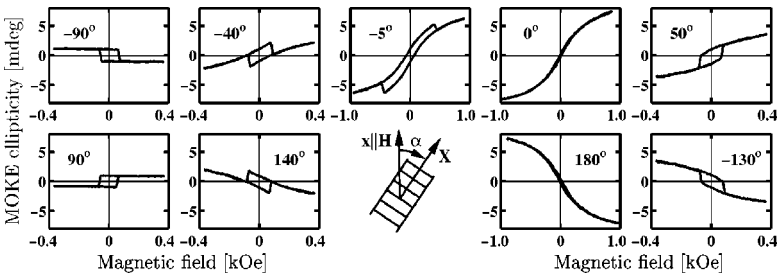

FIG. 4. Variation of the *s*-MOKE ellipticity loops measured at normal incidence angle in a transverse magnetic field $\mathbf{H}\|\hat{x}$, with sample rotation $\alpha=(\mathbf{H},\hat{X})$ around $\hat{n}$.

to the film. A small remanent signal is then measured as a consequence of the weakly tilted spin configuration with respect to the film plane by an angle γ_0. From the ratio between the remanent (1.1 mdeg) to saturated (46 mdeg) PMOKE amplitudes, one deduces $\gamma_0=1.4°$. Figure 4 shows MOKE ellipticity hysteresis loops always at normal incidence $\varphi=0$, but in a transverse magnetic field ($\mathbf{H}\|\hat{x}$), for several values of sample orientation α. Pure square loops were obtained for H applied along $\hat{Y}$ ($\alpha=\pm 90°$). They are only due to PMOKE, since both LMOKE, measured for $\varphi=0$ and VISMOKE [$\beta=0$ at saturation and hence $\cos(\alpha-\beta)=0$] are vanishing in this configuration. The PMOKE effect arises from the slight out-of-plane tilt of the easy axis by an angle γ_0 which may be estimated again to $\gamma_0=1.4°$ from the ratio between this PMOKE remanent (1.1 mdeg) signal and its value (46 mdeg) at saturation (for $\mathbf{H}\|\hat{n}$). Note the relative independence of the MOKE signal with $\mathbf{H}$ for $\alpha=\pm 90°$ in the $0.1<H<0.35$ kOe interval. Nevertheless, we checked that the signal tends to vanish at higher field (2.3 kOe). So, as expected, γ is decreasing from γ_0 towards zero for large in-plane field. Note that PMOKE should cancel in the presence of two equivalent anisotropy axes tilted by $\gamma_0=\pm 1.4°$, a situation expected in the case of a pure mirror symmetry. In our case, another small structural perturbation clearly lifts this degeneracy and, experimentally, only one easy axis survives. The scanning tunnel microscope (STM) image of the Au(322) vicinal surface [Fig. 2(a)] shows that the sample is slightly disoriented in azimuth with respect to the $[2\bar{1}1]$ direction, and therefore displays atomic kinks [see zoom in Fig. 2(a)] always oriented in the same direction. This effect explains such an additional symmetry breaking. The absence of a second easy axis is confirmed by the similarity of the hysteresis loops exhibited for a slight out-of-plane tilt of the external transverse magnetic field. The hysteresis loops, measured in transverse geometry ($\mathbf{H}\|\hat{x}$), and for several sample orientation angles α (Fig. 4), can be decomposed into square and S-shape contributions. Recall that $\varphi=0$ measured square hysteresis loops come only from PMOKE because of the residual out-of-plane component of $\mathbf{M}$. The variation of PMOKE with α is depicted on Fig. 5. The absolute value of the MOKE amplitude remains nearly constant under rotation of the sample around $\hat{n}$, which means that $\gamma\approx\gamma_0$ whatever the spin reorientation is in the plane. A residual field-dependent effect can be due to the distribution of step orientations or misalignment of the applied field ($<2°$). In agreement with an uniaxial anisotropy model,[13] the coercive field varies as $1/\sin\alpha$ and diverges at $\alpha=0°$ or 180°, i.e., when $\mathbf{H}$ becomes perpendicular to the step edges (Fig. 6).

The second contribution to MOKE ellipticity is the S-shape field-induced VISMOKE signal. The dependence of its amplitude with α is presented in Fig. 5. It reaches a maximum, far greater than the square loop magnitude, when the magnetization is saturated perpendicularly to the step edges, i.e., for $(\alpha-\beta)=0$ or 180° (see Fig. 4: loops corresponding to 0° or 180°) and vanishes for field $\mathbf{H}$ applied along the step edges [$(\alpha-\beta)=90°$] (see Fig. 4: loops corresponding to ±90°). As predicted theoretically for $\beta=0$, its amplitude varies with sample rotation as $\cos\alpha$. The low mirror symmetry of the staircase fixes a 2π periodicity for VISMOKE, i.e., it reverses sign when rotating the sample by 180° around $\hat{n}$ (Figs. 4 and 5).

The small dependence of γ with the applied field can be also checked from the $\alpha=0$ VISMOKE S-shape signal which exhibits a maximum at $\mathbf{H}\|\hat{x}=1.1$ kOe and saturates to a slightly lower value in higher field. The signal has already shown its full decrease, with a value of about 1.3 mdeg for

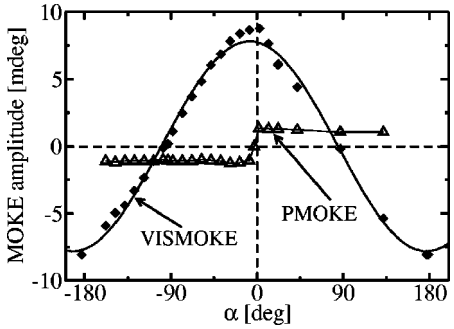

FIG. 5. Dependence of the ($\varphi=0$) *s*-MOKE ellipticity for the S-shape and square loop contributions as a function of the sample rotation α. The S-shape contribution is fitted by a cosine function.

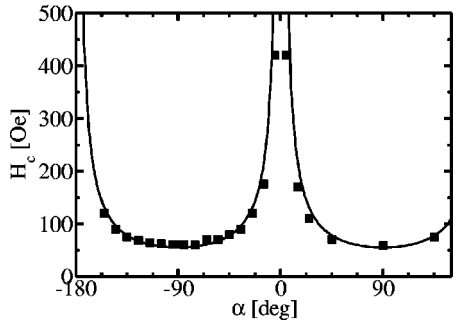

FIG. 6. Variation of the in-plane coercive field with the sample rotation angle α measured from the step orientation at $\mathbf{H}\|\hat{x}$. The full line shows fit with the function $H_c=H_{c0}/|\sin\alpha|$, $H_{c0}=55$ Oe.

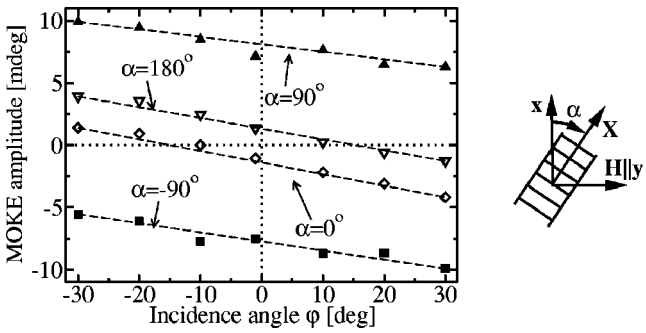

FIG. 7. Variation of the MOKE ellipticity amplitude of the square loop ($\alpha=0°$ and 180°) and S-shape ($\alpha=\pm 90°$) contributions with the incidence angle φ at $\mathbf{H}\|\hat{y}$.

2.3 kOe (our maximum field). Thus γ can be considered as field independent during the in-plane reorientation at low field in spite of the rather large miscut angle $\psi=11.4°$.

As shown above, the field-induced MOKE ($\mathbf{H}\|\hat{y}$) hysteresis curves can be decomposed into S-shape and square loop contributions. The dependence of the S-shape magnitude with the incidence angle φ, for sample orientations $\alpha=\pm 90°$, is presented in Fig. 7. Despite previous discussion, here $\mathbf{H}\|\hat{y}$ and thus the maximum of the S-shape signal is obtained for $\alpha=\pm 90°$. Associated variations of the square loop magnitude obtained for $\alpha=0$, 180° are also shown. As expected from Eq. (5), PMOKE and VISMOKE are quasiconstant while LMOKE varies quasilinearly with φ in the $\langle -30°, 30°\rangle$ interval. Since LMOKE is zero at normal incidence, we can extract the PMOKE and VISMOKE effects from the square loop and S-shape contributions at $\varphi=0$, respectively. As expected, the variation $\mathrm{Im}[d(\mathrm{MOKE})/d\varphi]=-0.078$ mdeg/° is identical in all cases (Fig. 7).

The VISMOKE maximum amplitude at $\alpha=0$, $\varrho_s t_s A\varepsilon_s\varepsilon_m/\varepsilon_d$, is found to be equal to $(0-9i)$ mdeg at saturation, although the saturated PMOKE amplitude for $\mathbf{H}\|\hat{n}$ ($\gamma=90°$), $\varrho_s t_{\mathrm{Co}} A\varepsilon_m$, is $(-23+48i)$ mdeg. From the VISMOKE/PMOKE ratio, we deduce $\varepsilon_s t_s/\varepsilon_d t_{\mathrm{Co}}=(-0.15+0.07i)\pm 0.02$ mdeg. Assuming $t_s=2$ AL and using the diagonal Co permittivity $\varepsilon_d=-12.6+18.5i$, we deduce a rather large value $\varepsilon_s=1.42-9.38i$ for the optostructural coefficient.

V. OPTICAL DETERMINATION OF ε_s

The value of $\varepsilon_s t_s/\varepsilon_d t_{\mathrm{Co}}$ has been confirmed independently from differential reflectivity measurements. Since $\varepsilon_{xz}=\varepsilon_s\cos\alpha$ and $\varepsilon_{yz}=\varepsilon_s\sin\alpha$ and as follows from Eqs. (3) and (5), one finds a vicinal Kerr *p*-structural contribution $\Phi_p^{(\mathrm{struc})}$,

$$\Phi_p^{(\mathrm{struc})}=\tfrac{1}{2}\rho_p t_s A\varepsilon_s^2/\varepsilon_d\sin 2\alpha+\rho_p t_s B\varepsilon_s/\varepsilon_d\cos\alpha, \quad (7)$$

and analogously for the Kerr *s*-effect. The first term in Eq. (7) is "structural VISMOKE," the second one "structural LMOKE." There is no "structural PMOKE," as ε_{xy}, ε_{yx} does not depend on ε_s [see Eq. (3)]. Thus, in principle, it is possible to determine ε_s by varying α, i.e., rotating the film around its normal axis. However, in order to get a better accuracy on ε_s, we preferred to keep the sample fixed and rotate all optical elements by an angle μ. By this way, the reflected light beam is surely fixed in position through all optical elements. For structural determination of ε_s we used an optical setup with the following arrangement: laser–polarizer–photoelastic modulator–sample–detector, in the spirit of linear birefringence setup.[14] The measured signal found at frequency 2ω (ω being the modulator frequency) for $\mu=0$ is

$$S=I_{2\omega}/I_0=(|r_{ss}|^2-|r_{pp}|^2)/(|r_{ss}|^2+|r_{pp}|^2).$$

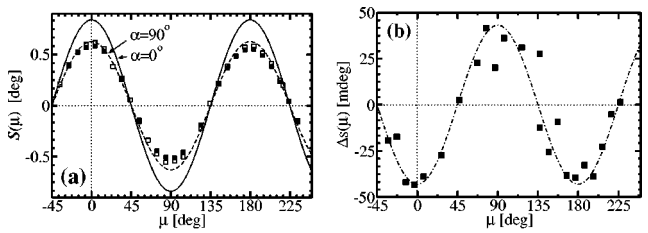

FIG. 8. (a) Variation of the differential optical reflectivity $S=(|r_{ss}|^2-|r_{pp}|^2)/(|r_{ss}|^2+|r_{pp}|^2)$, measured for $\alpha=0°$ (□) and $\alpha=90°$ (■) as a function of the orientation angle μ of the optical elements with respect to the sample. The calculated $S(\mu)\sim\cos 2\mu$ curves are represented by lines. (b) The difference $\Delta S(\mu)=S_{\alpha=90°}(\mu)-S_{\alpha=0°}(\mu)$ is related to ε_s^2. The dash-dotted line represents the $-\cos 2\mu$ variation and stands as a guide for the eye.

When the optical elements are rotated by angle μ, the reflection coefficients are replaced by $r'_{ss}=r_{ss}\cos^2\mu-r_{pp}\sin^2\mu$ and $r'_{pp}=r_{pp}\cos^2\mu-r_{ss}\sin^2\mu$. The large contributions to reflectivity signal $S(\mu)$, which are not linked to ε_s, cancel out by subtracting two successive measurements performed for $\alpha=0$ and $\alpha=90°$, leading to

$$\Delta S(\mu)=S_{\alpha=90°}-S_{\alpha=0}\approx-\frac{2\,\mathrm{Re}\{\varepsilon_s^2[\rho_{ss}^{(2)}(r_{ss}^{(0)})^\dagger+\rho_{pp}^{(2)}(r_{pp}^{(0)})^\dagger]\}}{|r_{ss}^{(0)}|^2+|r_{pp}^{(0)}|^2}t_s\cos 2\mu, \quad (8)$$

where † means complex conjugation. We used

$$r_{ss}=r_{ss}^{(0)}+\rho_{ss}^{(2)}t_s\varepsilon_s^2\cos^2\alpha$$

and

$$r_{pp}=r_{pp}^{(0)}+\rho_{pp}^{(2)}t_s\varepsilon_s^2\sin^2\alpha,$$

where $r_{ss}^{(0)}$, $r_{pp}^{(0)}$ and $\rho_{pp}^{(2)}$, $\rho_{ss}^{(2)}$ are zero and second-order diagonal reflection coefficients in ε_{ij}, with $i\neq j$, respectively, presented in the Appendix. Notice that ΔS does not depend much on r_{sp}, r_{ps} at $\varphi=30°$, thus the dependence of ΔS on ε_s is only related to $\rho_{ss}^{(2)}$, $\rho_{pp}^{(2)}$, leading to $\Delta S\sim\varepsilon_s^2$. Experimental data relative to the $S(\mu)$ variations of a sample in its remnant state at $\varphi=30°$, for $\alpha=0°$ and 90°, and of their difference $\Delta S(\mu)$ are represented on Fig. 8. The experimentally deduced differential curve [Fig. 8(b)] exhibits a $C\cos 2\mu$ dependence with $C=40$ mdeg. In counterpart, substituting the complex value of ε_s obtained from MOKE mea-

TABLE I. Reflection coefficients for a sandwiched ultrathin FM layer. For discussion of this table see the Appendix.

r_{ps}		$\frac{2i\eta t_{\rm fm}\, QN_0\cos\varphi}{(N_0\cos\varphi+N_z)[N_0N_z+(N_{\rm nf})^2\cos\varphi]}\left[\frac{\varepsilon_{zx}\varepsilon_{yz}N_z}{\varepsilon_d}-\frac{\varepsilon_{zx}N_y(N_{\rm nf})^2}{\varepsilon_d}-\varepsilon_{yx}N_z\right]$
r_{sp}		$\frac{2i\eta t_{\rm fm}\, QN_0\cos\varphi}{(N_0\cos\varphi+N_z)[N_0N_z+(N_{\rm nf})^2\cos\varphi]}\left[-\frac{\varepsilon_{xz}\varepsilon_{zy}N_z}{\varepsilon_d}-\frac{\varepsilon_{xz}N_y(N_{\rm nf})^2}{\varepsilon_d}+\varepsilon_{xy}N_z\right]$
r_{ss}	$r_{ss}^{(0)}$	$\frac{N_0\cos\varphi-N_z}{N_0\cos\varphi+N_z}$
	$r_{ss}^{(0,\eta)}=\rho_{ss}^{(0,\eta)}t_{\rm fm}$	$\frac{2i\eta QN_0\cos\varphi[\varepsilon_d-(N_{\rm nf})^2]}{(N_0\cos\varphi+N_z)^2}t_{\rm fm}$
	$r_{ss}^{(2)}=\rho_{ss}^{(2)}t_{\rm fm}\varepsilon_{xz}\varepsilon_{zx}$	$-\frac{2i\eta QN^{(0)}\cos\varphi}{\varepsilon_d(N^{(0)}\cos\varphi+N_z)^2}t_{\rm fm}\varepsilon_{xz}\varepsilon_{zx}$
r_{pp}	$r_{pp}^{(0)}$	$\frac{(N_{\rm nf})^2\cos\varphi-N_zN_0}{(N_{\rm nf})^2\cos\varphi+N_zN_0}$
	$r_{pp}^{(0,\eta)}=\rho_{pp}^{(0,\eta)}t_{\rm fm}$	$-\frac{2i\eta QN_0\cos\varphi[-(N_{\rm nf})^4(\varepsilon_d-(N_y)^2)+(N_z)^2(\varepsilon_d)^2]}{\varepsilon_d[N_0N_z+(N_{\rm nf})^2\cos\varphi]^2}t_{\rm fm}$
	$r_{pp}^{(1)}=\rho_{pp}^{(1)}t_{\rm fm}(\varepsilon_{yz}-\varepsilon_{xy})$	$+\frac{2i\eta Q(N_{\rm nf})^2N_yN_zN_0\cos\varphi}{\varepsilon_d[N_0N_z+(N_{\rm nf})^2\cos\varphi]^2}t_{\rm fm}(\varepsilon_{yz}-\varepsilon_{zy})$
	$r_{pp}^{(2)}=\rho_{pp}^{(2)}t_{\rm fm}\varepsilon_{yz}\varepsilon_{zy}$	$\frac{2i\eta Q(N_z)^2N_0\cos\varphi}{\varepsilon_d[N_0N_z+(N_{\rm nf})^2\cos\varphi]^2}t_{\rm fm}\varepsilon_{yz}\varepsilon_{zy}$

surements and again assuming $t_s=2$ AL, we deduce $C=210$ mdeg. So, since $\Delta S(\mu)\sim\varepsilon_s^2$, optical measurements give approximately half the value of ε_s given by the VISMOKE/PMOKE ratio. Maximum measurement and calibration errors could be $\approx$20%; thus this cannot explain the discrepancy between MOKE and optical determinations of ε_s. This can be explained behind our simplified model assuming the step profiles of both ε_s (simplified thickness t_s) and ε_m (over thickness $t_{\rm fm}$). Taking into account the profiles of $\varepsilon_s(n)$ and $\varepsilon_m(n)$, different measurements give different integral informations,[15] i.e., VISMOKE is proportional to $\int\varepsilon_s(n)\varepsilon_m(n)dn$, PMOKE to $\int\varepsilon_m(n)dn$ and $\Delta S\sim\int\varepsilon_s^2(n)dn$.

VI. SIMPLE PHENOMENOLOGICAL MODEL OF ε_s

The microscopic origin of the optostructural perturbation ε_s can be associated to the difference between electronic band structures for vicinal and planar interfaces. Another contribution comes from the different boundary conditions of the electrical field at vicinal or planar interfaces. The simple phenomenological model we propose assumes that the classical boundary conditions are not fulfilled if considering the mean optical plane of the vicinal interface, but are only valid for each step tilted from this plane by the miscut angle ψ [see Fig. 1(a)]. Then, the boundary conditions between two isotropic media (a) and (b), separated by a vicinal interface may be expressed by

$$\Delta\mathbf{D}^{(\rm vic)}=\mathbf{D}^{(b,\rm vic)}-\mathbf{D}^{(a,\rm vic)}=(\varepsilon_d^{(b)}-\varepsilon_d^{(a)})\times\begin{bmatrix}E_x^{(a)}\cos^2\psi+\frac{1}{2}E_z^{(a)}\sin 2\psi\\ E_y^{(a)}\\ \frac{1}{2}E_x^{(a)}\sin 2\psi+E_z^{(a)}\sin^2\psi\end{bmatrix},\qquad(9)$$

where $\varepsilon_d^{(a)}$, $\varepsilon_d^{(b)}$ are the diagonal permittivity tensor elements of the (a), (b) media, respectively. In order to restore usual boundary conditions at long range we choose to express the difference between step boundary conditions and those given by a planar interface $\Delta\mathbf{D}^{(\rm pln)}=\mathbf{D}^{(b,\rm pln)}-\mathbf{D}^{(a,\rm pln)}=(\varepsilon_d^{(b)}-\varepsilon_d^{(a)})[E_x^{(a)};E_y^{(a)};0]$ by a modification of the permittivity tensor in the close vicinity of the vicinal interface; this leads to nonzero off-diagonal permittivity elements. Assuming that the difference between planar and vicinal boundary conditions $\Delta\mathbf{D}^{(\rm vic)}-\Delta\mathbf{D}^{(\rm pln)}$ is equally distributed between both media (a) and (b), we obtain structural off-diagonal permittivity element in (a) material

$$\varepsilon_s^{(a)}=\tfrac{1}{4}(\varepsilon_d^{(b)}-\varepsilon_d^{(a)})\sin 2\psi.\qquad(10)$$

This result can be applied to both types of area of vicinal interfaces, denoted on Fig. 1(a) as (l) and (s) and having orientations ψ and $\psi-90°$, respectively. Substituting these angles onto Eq. (10), we found that these contributions (per unit area) give opposite sign for ε_s. Thus, suming weighted contributions from (s) and (l) area, we arrive at

$$\varepsilon_s^{(a)}=\tfrac{1}{4}(\varepsilon_d^{(b)}-\varepsilon_d^{(a)})(\cos^2\psi-\sin^2\psi)\sin 2\psi.\qquad(11)$$

In the case of a small miscut angle ψ, the (s) area is much smaller than the (l) area and the contribution from (s) area can be neglected. Thus, considering only the (l) area, ε_s expresses by Eq. (10). In the case of $\psi=45°$, Eq. (11) leads to $\varepsilon_s=0$, as expected when new mirror plane symmetry appears. In the case of Co deposited on Au(322), Eq. (11) leads to $\varepsilon_s=-0.09-1.67i$. From this simple model about 18% of the experimental value can be accounted for. To get a more quantitative agreement, refined calculations taking account of the influence of the modified boundary conditions and the perturbation on the electronic band structure are required. From an experimental point of view, the spectral dependence of ε_s can give some insight into the processes involved at the vicinal interface.

VII. CONCLUSION

VISMOKE has been analytically predicted and evidenced in a Co film deposited on a Au(322) vicinal surface, but it is always expected for ferromagnetic films deposited on low-symmetry surfaces, (i.e., surfaces providing only one mirror plane symmetry). Obviously, VISMOKE is never present in a Co film grown on a high-symmetry surface, such as Au(111). VISMOKE can provide a new way to investigate selectively the magnetic behavior and magneto-optical spectroscopy of interfaces. Magneto-optics on the second harmonic generation of light can also be used for the same purpose, but the possible investigated spectral range is up to now too limited to compete with VISMOKE spectroscopy. VISMOKE comes from the interference between the opto-structural perturbation ε_s induced by the lowering of interface symmetry and the usual magneto-optical perturbation ε_m. It is characterized by a 2π symmetry behavior when rotating the film around its normal axis. A phenomenological origin of ε_s has been proposed, predicting a linear variation of the VISMOKE with the degree of vicinality for small miscut angles. As experimentally demonstrated, VISMOKE has to be considered in all MOKE studies relative to FM films grown on vicinal surfaces.

APPENDIX

Reflection coefficients for an ultrathin FM layer sandwiched between an infinite substrate and an overlayer of thickness t_{over} are presented in Table I. The term $\eta=2\pi/\lambda_0$ is the vacuum wave vector and $Q=\exp[4\pi i N_z t_{\text{over}}/\lambda_0]$ the influence of the overlayer. The other terms are defined inside the text. The total reflection coefficients are given by a sum of partial contributions, $r_{ss}=r_{ss}^{(0)}+r_{ss}^{(0,\eta)}+r_{ss}^{(2)}$ and similarly for r_{pp}; the superscripts$^{(0)}$,$^{(1)}$,$^{(2)}$ denote the order of perturbation of the off-diagonal permittivity coefficients ε_{ij}, $i\neq j$, of the FM layer. Table I gives all contributions to reflection coefficients at first order of Fourier transformation by t_{fm}, i.e., when $r_{ij}=a+bt_{\text{fm}}$, where $i, j=\{s,p\}$.

ACKNOWLEDGMENTS

We would like to thank B. Hillebrands for stimulating discussions on this subject. One of us (J.H.) would like to thank the Ministère Français des Affaires Étrangères for the financial support of his stay in France. The CNRS has supported this work through a contract on Material Science.

*Corresponding author. Electronic address: ferre@lps.u-psud.fr

[1] For a general review, see *Ultrathin Magnetic Structures I and II*, edited by B. Heinrich and J. A. C. Bland (Springer-Verlag, Berlin, 1994).
[2] J. Shen and J. Kirschner, Surf. Sci. **500**, 300 (2002).
[3] A. Kirilyuk, J. Phys. D **35**, R189 (2002).
[4] R. Nakajima, J. Stöhr, and Y. U. Idzerda, Phys. Rev. B **59**, 6421 (1999).
[5] R. K. Kawakami, E. Escorcia-Aparicio, and Z. Qiu, Phys. Rev. Lett. **77**, 2570 (1996).
[6] P. Haibach, M. Huth, and H. Adrian, Phys. Rev. Lett. **84**, 1312 (2000).
[7] A. Hubert and R. Schafer, *Magnetic Domains* (Springer, Berlin, 1998).
[8] S. Visnovsky, M. Nývlt, V. Prosser, R. Lopušník, R. Urban, J. Ferré, G. Pénissard, J. P. Renard, and R. Krishnan, Phys. Rev. B **52**, 1090 (1995).
[9] A. Pethukov, A. Kirilyuk, and T. Rasing, Phys. Rev. B **59**, 4211 (1999).
[10] L. Landau and E. Lifchitz, *Electrodynamics of Continuous Media* (Edition Mir, Moscau, 1969).
[11] R. Birss, *Symmetry and Magnetism* (North-Holland, Amsterdam, 1964).
[12] V. Grolier, J. Ferré, A. Maziewski, E. Stefanowicz, and D. Renard, J. Appl. Phys. **73**, 5939 (1993).
[13] E. Kondorsky, J. Phys. (Moscow) **2**, 161 (1940).
[14] J. Ferré and G. A. Gehring, Rep. Prog. Phys. **47**, 513 (1984).
[15] J. Hamrle, M. Nývlt, Š. Višňovský, P. Beauvellain, R. Mégy, J. Ferré, L. Polerecký, and D. Renard, Phys. Rev. B **64**, 155405 (2001).